Eur. Phys. J. B **4**, 285–289 (1998)

THE EUROPEAN PHYSICAL JOURNAL B

Long and short range spin-spin interactions in $ErBa_2Cu_3O_7$

E. Rastelli[a] and A. Tassi

Dipartimento di Fisica and Istituto Nazionale per la Fisica della Materia, Università di Parma, 43100 Parma, Italy

Received: 12 January 1998 / Received in final form: 26 March 1998 / Accepted: 10 April 1998

Abstract. Dipolar spin-spin interactions play a crucial role as for the magnetic order in the compounds of the $RBa_2Cu_3O_{6+x}$ family, (R = Dy, Er, Nd). However, inelastic neutron scattering data observed in $ErBa_2Cu_3O_7$ can be explained only if exchange interactions in addition to dipolar ones are taken into account.

PACS. 75.10.-b General theory and models of magnetic ordering – 75.25.+z Spin arrangements in magnetically ordered materials (including neutron and spin-polarized electron studies, synchrotron-source X-ray scattering, etc.) – 75.50.-y Studies of specific magnetic materials

1 Introduction

Rare earth compounds of the $RBa_2Cu_3O_{6+x}$ (R = Dy, Er, Nd) family are extensively studied [1] and the main part of the observed spin configurations of the rare earth ions lattice are *columnar* with alternating ferromagnetic chains. Magnetic long range order disappears above a very low critical temperature (T_N <1 K). In particular the Er^{3+} ions in $ErBa_2Cu_3O_7$ localized on an orthorhombic lattice with $a = 3.82$ Å, $b = 3.88$ Å, $c = 11.66$ Å below $T_N = 0.6$ K show long range antiferromagnetic order along a and c, and ferromagnetic order along b characterized by the wave vector $\mathbf{Q} = (\frac{1}{2}, 0, \frac{1}{2})$ with spins pointing along b [1]. This spin configuration is ascribed to dipolar interactions [1], but in presence of *only* dipolar forces characterized by $g_{xx} = g_{yy}$ spins make ferromagnetic chains along a ($\mathbf{Q} = (0, \frac{1}{2}, \frac{1}{2})$) and spins point along a [2] in contrast with experiment. Indeed in equation (3.3) of reference [2] one sees that the configuration corresponding to an order wave vector $\mathbf{Q} = (0, \frac{1}{2}, \frac{1}{2})$ with spins pointing along a has a lower dipolar energy with respect to the configuration corresponding to $\mathbf{Q} = (\frac{1}{2}, 0, \frac{1}{2})$ with spins pointing along b. However, suitable exchange interactions can stabilize the $\mathbf{Q} = (\frac{1}{2}, 0, \frac{1}{2})$ configuration [2]. On the other hand a Heisenberg model with *only* exchange interactions [3] supports the spin configuration observed by elastic neutron scattering and the spin wave spectrum too agrees with experimental data obtained by inelastic neutron scattering [4]. Anyway a reliable picture cannot neglect dipolar forces. Indeed long time ago [5] it was shown that the dipolar interaction contribution to the elementary excitation spectrum can be simulated by a single ion effective anisotropy in transition metal compounds where the exchange interaction is sufficiently large. This is not the case for $ErBa_2Cu_3O_7$ where the exchange coupling is very weak.

Moreover the energy level scheme for Er^{3+} ions in $ErBa_2Cu_3O_x$ ($6 < x < 7$) was investigated by neutron spectroscopy and fitted by crystalline-electric-field (CEF) calculation [6]. This calculation leads to a Kramers doublet ground state corresponding to an effective spin $S = 1/2$ with an anisotropic diagonal g-tensor ($g_{xx} \neq g_{yy} \neq g_{zz}$). The in-plane anisotropy ($g_{xx} \neq g_{yy}$) is sufficient to stabilize the spin configuration observed in $ErBa_2Cu_3O_7$ even though exchange interactions are neglected. However, we find that the magnon spectrum obtained from inelastic neutron scattering can be recovered only if nearest neighbour (NN) and next nearest neighbour (NNN) exchange interactions are accounted for.

In Section 2 we evaluate the g-factors of the Er^{3+} ions assuming the CEF parameters suggested in reference [6] and we study the region of stability of the observed spin configuration in $ErBa_2Cu_3O_7$ when both dipolar and exchange interactions are accounted for. In Section 3 we work out the spin wave spectrum and we find a relevant splitting of the spin wave dispersion curve not observed in experiment [4]. In Section 4 we give the inelastic neutron scattering cross-section and show that the observation of only one spin wave branch could be ascribed to different intensities of the two spin wave branches along with a limited instrument resolution.

2 Minimum energy spin configuration

Neutron spectroscopy of the energy levels of the Er^{3+} ions in $ErBa_2Cu_3O_x$ ($6 < x < 7$) was explained by CEF calculation [6]. The magnetic properties of the Er^{3+} ion at low temperature can be described by a localized effective spin $S = 1/2$ with an anisotropic g-tensor. On the basis

[a] e-mail: `rastelli@fisica.unipr.it` or `rastelli@pr.infn.it`

of the CEF parameters given in Table II of reference [6] for $ErBa_2Cu_3O_{6.98}$ we have evaluated the wave functions belonging to the ground state doublet and the matrix elements of the diagonal g-tensor. We obtain

$$g_{xx} = 7.42, \quad g_{yy} = 8.04, \quad g_{zz} = 4.57. \tag{2.1}$$

Anisotropy in the x and y components of the g-tensor was also predicted [7,8] by means of CEF theory on the basis of scaled inelastic neutron scattering results for $HoBa_2Cu_3O_7$. Anyway we base our calculations on the level scheme of Er^{3+} ions calculated by the CEF theory using experimental data of inelastic neutron scattering on $ErBa_2Cu_3O_7$ [6]. We evaluate the classical energies of the collinear spin configurations in an orthorhombic lattice starting from the following Hamiltonian model

$$\begin{aligned}\mathcal{H} =&\frac{1}{2}\mu_B^2 \sum_{\alpha,\beta}\sum_{i,\mathbf{R}} \frac{1}{R^3}\Big(\delta_{\alpha,\beta} - 3\frac{R^\alpha R^\beta}{R^2}\Big) g_{\alpha\alpha} g_{\beta\beta} S_i^\alpha S_{i+\mathbf{R}}^\beta \\ &+ \eta_x \sum_{i,\boldsymbol{\delta}} J_{\boldsymbol{\delta}} S_i^x S_{i+\boldsymbol{\delta}}^x + \sum_{i,\boldsymbol{\delta}} J_{\boldsymbol{\delta}} S_i^y S_{i+\boldsymbol{\delta}}^y + \eta_z \sum_{i,\boldsymbol{\delta}} S_i^z S_{i+\boldsymbol{\delta}}^z\end{aligned} \tag{2.2}$$

where $\alpha, \beta = x, y, z$, μ_B is the Bohr magneton, i, and $\mathbf{R}$ label the sites of an orthorhombic lattice. $J_{\boldsymbol{\delta}}$ is J for $\boldsymbol{\delta} = (\pm a, 0, 0), (0, \pm b, 0)$, J' for $\boldsymbol{\delta} = (0, 0, \pm c)$, and J_2 for $\boldsymbol{\delta} = (\pm a, \pm b, 0)$. $2J$, $2J'$ and $2J_2$ are the NN in plane, NN out of plane, and NNN in plane antiferromagnetic exchange couplings, respectively. The exchange anisotropy constants are assumed to be $\eta_x = (g_{xx}/g_{yy})^2 = 0.85$, $\eta_z = (g_{zz}/g_{yy})^2 = 0.32$.

The classical energy of the model Hamiltonian (2.2) for collinear spin configurations can be characterized by a wave vector $\mathbf{Q}$ and polar angles θ and ϕ of the spins with respect to the crystal axis x, y, z pointing along a, b, c, respectively.

$$\begin{aligned}E_0(\mathbf{Q}) =&\frac{1}{2}NS(S+1)\Big\{\big[-\mu_B^2 g_{xx}^2 D^{xx}(\mathbf{Q}) \\ &+ 2\eta_x J(\mathbf{Q})\big]\sin^2\theta\cos^2\phi + \big[-\mu_B^2 g_{yy}^2 D^{yy}(\mathbf{Q}) \\ &+ 2J(\mathbf{Q})\big]\sin^2\theta\sin^2\phi \\ &+ \big[-\mu_B^2 g_{zz}^2 D^{zz}(\mathbf{Q}) + 2\eta_z J(\mathbf{Q})\big]\cos^2\theta\Big\}\end{aligned} \tag{2.3}$$

where

$$D^{\alpha\beta}(\mathbf{Q}) = \sum_{\mathbf{R}} \frac{1}{R^3}\Big(3\frac{R^\alpha R^\beta}{R^2} - \delta_{\alpha\beta}\Big) e^{-i\mathbf{Q}\cdot\mathbf{R}} \tag{2.4}$$

and

$$\begin{aligned}J(\mathbf{Q}) =& 2J[\cos(aQ_x) + \cos(bQ_y)] \\ &+ 2J'\cos(cQ_z) + 4J_2\cos(aQ_x)\cos(bQ_y).\end{aligned} \tag{2.5}$$

Dipolar interactions and NNN exchange interaction J_2 select *columnar* spin configurations whereas NN exchange interaction J supports Néel configurations. Note that possible ferromagnetic order along the c-axis is ruled out by the antiferromagnetic exchange coupling J'. So we study the spin configurations which have the lowest energy in presence of antiferromagnetic exchange interactions. These configurations are characterized by the wave vectors $\mathbf{Q} = (0, \frac{1}{2}, \frac{1}{2})$, $\mathbf{Q} = (\frac{1}{2}, 0, \frac{1}{2})$ and $\mathbf{Q} = (\frac{1}{2}, \frac{1}{2}, \frac{1}{2})$ for which the classical energies (in meV) are

$$\begin{aligned}E_0\Big(0, \frac{1}{2}, \frac{1}{2}\Big) =&\frac{1}{2}S(S+1)N\Big\{-\big[0.004881 g_{xx}^2 \\ &+ 4\eta_x(J' + 2J_2)\big]\sin^2\theta\cos^2\phi \\ &+ \big[0.005673 g_{yy}^2 - 4(J' + 2J_2)\big]\sin^2\theta\sin^2\phi \\ &- \big[0.000792 g_{zz}^2 + 4\eta_z(J' + 2J_2)\big]\cos^2\theta\Big\}.\end{aligned} \tag{2.6}$$

The minimum is obtained for $\theta = \pi/2, \phi = 0$ corresponding to the $q(6x)$ configuration in the notation of reference [2].

$$\begin{aligned}E_0\Big(\frac{1}{2}, 0, \frac{1}{2}\Big) =&\frac{1}{2}S(S+1)N\Big\{\big[0.005671 g_{xx}^2 \\ &- 4\eta_x(J' + 2J_2)\big]\sin^2\theta\cos^2\phi \\ &- \big[0.004715 g_{yy}^2 + 4(J' + 2J_2)\big]\sin^2\theta\sin^2\phi \\ &- \big[0.000956 g_{zz}^2 + 4\eta_z(J' + 2J_2)\big]\cos^2\theta\Big\}.\end{aligned} \tag{2.7}$$

The minimum is obtained for $\theta = \pi/2, \phi = \pi/2$ corresponding to the $q(8y)$ configuration in the notation of reference [2]. Note that for an in-plane *isotropic* g-tensor ($g_{xx} = g_{yy} = g_\perp$) and $\eta_x = 1$ the $\mathbf{Q} = (\frac{1}{2}, 0, \frac{1}{2})$ configuration is unstable with respect to the $\mathbf{Q} = (0, \frac{1}{2}, \frac{1}{2})$ configuration in agreement with equation (3.3) of reference [2].

$$\begin{aligned}E_0\Big(\frac{1}{2}, \frac{1}{2}, \frac{1}{2}\Big) =& \frac{1}{2}S(S+1)N\Big\{\big[0.001394 g_{xx}^2 \\ &- 4\eta_x(2J + J' - 2J_2)\big]\sin^2\theta\cos^2\phi \\ &+ \big[0.001096 g_{yy}^2 - 4(2J + J' - 2J_2)\big]\sin^2\theta\sin^2\phi \\ &- \big[0.002490 g_{zz}^2 + 4\eta_z(2J + J' - 2J_2)\big]\cos^2\theta\Big\}.\end{aligned} \tag{2.8}$$

The minimum is obtained for $\theta = 0$ corresponding to the $q(2z)$ configuration in the notation of reference [2].

We find the $\mathbf{Q} = (\frac{1}{2}, 0, \frac{1}{2})$ configuration observed in $ErBa_2Cu_3O_7$ [1] to be stable when $J - 2J_2 < 0.00073 g_{yy}^2 = 0.047$ meV.

3 Spin waves

To get the spin wave spectrum [9] we perform a transformation from the x, y, z crystal axis to local axis ξ, η, ζ where ζ (the local quantization axis) is parallel to y. The local axis are modulated according to the order wave vector $\mathbf{Q}$. Note that $2\mathbf{Q}$ is a reciprocal lattice vector for

all collinear spin configurations. We perform the customary spin-boson transformation retaining only the contributions that give the bilinear part of the Hamiltonian:

$$S_i^x = -\cos(\mathbf{Q}\cdot\mathbf{r}_i)\frac{\sqrt{2S}}{2i}(a_i - a_i^\dagger) \tag{3.1}$$

$$S_i^y = \cos(\mathbf{Q}\cdot\mathbf{r}_i)(S - a_i^\dagger a_i) \tag{3.2}$$

$$S_i^z = -\frac{\sqrt{2S}}{2}(a_i + a_i^\dagger). \tag{3.3}$$

Substitution of (3.1, 3.2, 3.3) in Hamiltonian (2.2) leads to the following bilinear Hamiltonian

$$\mathcal{H}_2 = \sum_{\mathbf{q}} \Big\{ A_{\mathbf{q}} a_{\mathbf{q}}^\dagger a_{\mathbf{q}} + \frac{1}{2} B_{\mathbf{q}} (a_{\mathbf{q}} a_{-\mathbf{q}} + a_{\mathbf{q}}^\dagger a_{-\mathbf{q}}^\dagger) + \frac{1}{2}(iC_{\mathbf{q}} a_{\mathbf{q}} a_{-\mathbf{q}-\mathbf{Q}} - iC_{\mathbf{q}} a_{\mathbf{q}}^\dagger a_{-\mathbf{q}-\mathbf{Q}}^\dagger) + iD_{\mathbf{q}} a_{\mathbf{q}}^\dagger a_{\mathbf{q}+\mathbf{Q}} \Big\} \tag{3.4}$$

where

$$\begin{aligned} A_{\mathbf{q}} =& \frac{1}{2}\mu_B^2 S\big[2g_{yy}^2 D^{yy}(\mathbf{Q}) \\ & - g_{xx}^2 D^{xx}(\mathbf{q}+\mathbf{Q}) - g_{zz}^2 D^{zz}(\mathbf{q})\big] \\ & + 2S\big\{2J' + 4J_2 - \eta_x[J(\cos(aq_x) - \cos(bq_y)) \\ & + J'\cos(cq_z) + 2J_2\cos(aq_x)\cos(bq_y)] \\ & + \eta_z[J(\cos(aq_x) + \cos(bq_y)) \\ & + J'\cos(cq_z) + 2J_2\cos(aq_x)\cos(bq_y)]\big\} \end{aligned} \tag{3.5}$$

$$\begin{aligned} B_{\mathbf{q}} =& \frac{1}{2}\mu_B^2 S\big[g_{xx}^2 D^{xx}(\mathbf{q}+\mathbf{Q}) - g_{zz}^2 D^{zz}(\mathbf{q})\big] \\ & + 2S\big\{\eta_x[J(\cos(aq_x) - \cos(bq_y)) + J'\cos(cq_z) \\ & + 2J_2\cos(aq_x)\cos(bq_y)] \\ & + \eta_z[J(\cos(aq_x) + \cos(bq_y)) + J'\cos(cq_z) \\ & + 2J_2\cos(aq_x)\cos(bq_y)]\big\} \end{aligned} \tag{3.6}$$

$$C_{\mathbf{q}} = -\frac{1}{2}\mu_B^2 S g_{xx} g_{zz}\big[D^{xz}(\mathbf{q}) + D^{xz}(\mathbf{q}+\mathbf{Q})\big] \tag{3.7}$$

$$D_{\mathbf{q}} = -\frac{1}{2}\mu_B^2 S g_{xx} g_{zz}\big[D^{xz}(\mathbf{q}) - D^{xz}(\mathbf{q}+\mathbf{Q})\big]. \tag{3.8}$$

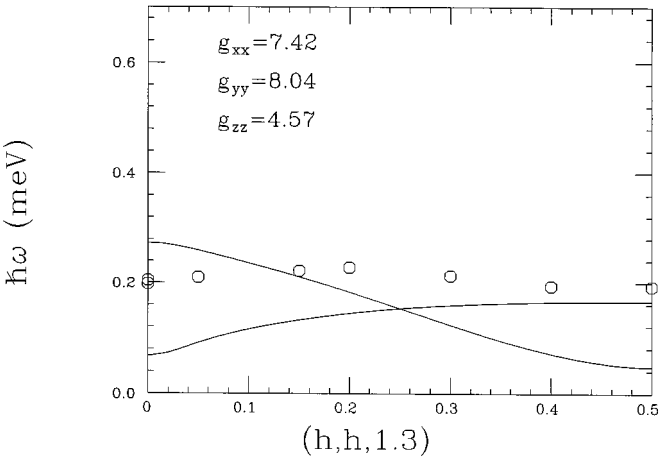

Fig. 1. Dispersion relation along $(h, h, 1.3)$ in r.l.u. taking only dipolar interactions into account. Open circles are experimental data from reference [4].

Diagonalization of (3.4) leads to the following two branches of the spin wave spectrum

$$\begin{aligned} \hbar\omega_{\mathbf{q}}^{\pm} =& \Bigg\{ \frac{1}{2}\Big[A_{\mathbf{q}}^2 - B_{\mathbf{q}}^2 + A_{\mathbf{q}+\mathbf{Q}}^2 - B_{\mathbf{q}+\mathbf{Q}}^2\Big] - \Big(C_{\mathbf{q}}^2 - D_{\mathbf{q}}^2\Big) \\ & \pm \Bigg[\frac{1}{4}\Big(A_{\mathbf{q}}^2 - B_{\mathbf{q}}^2 - A_{\mathbf{q}+\mathbf{Q}}^2 + B_{\mathbf{q}+\mathbf{Q}}^2\Big)^2 \\ & - C_{\mathbf{q}}^2\Big(\big(A_{\mathbf{q}} - A_{\mathbf{q}+\mathbf{Q}}\big)^2 - \big(B_{\mathbf{q}} - B_{\mathbf{q}+\mathbf{Q}}\big)^2\Big) \\ & + D_{\mathbf{q}}^2\Big(\big(A_{\mathbf{q}} + A_{\mathbf{q}+\mathbf{Q}}\big)^2 - \big(B_{\mathbf{q}} + B_{\boldsymbol{q}+\boldsymbol{Q}}\big)^2\Big) \\ & - 4C_{\mathbf{q}} D_{\mathbf{q}}\Big(A_{\mathbf{q}} B_{\mathbf{q}+\mathbf{Q}} - A_{\mathbf{q}+\mathbf{Q}} B_{\mathbf{q}}\Big)\Bigg]^{1/2}\Bigg\}^{1/2}. \end{aligned} \tag{3.9}$$

Similar spectra were obtained for 2D square lattice [10] as well as for hexagonal lattice [11] in order to describe the neutron scattering measurements on the ferromagnetic chain system $CsNiF_3$. For high symmetry directions one finds $C_{\mathbf{q}} = D_{\mathbf{q}} = 0$. In $ErBa_2Cu_3O_7$ we have proved that $C_{\mathbf{q}} \simeq D_{\mathbf{q}} \simeq 0$ for any $\mathbf{q}$. For this reason the spectra (3.9) reduce to

$$\hbar\omega_{\mathbf{q}}^{+} = \hbar\omega_{\mathbf{q}} = \sqrt{A_{\mathbf{q}}^2 - B_{\mathbf{q}}^2} \tag{3.10}$$

$$\hbar\omega_{\mathbf{q}}^{-} = \hbar\omega_{\mathbf{q}+\mathbf{Q}} = \sqrt{A_{\mathbf{q}+\mathbf{Q}}^2 - B_{\mathbf{q}+\mathbf{Q}}^2}. \tag{3.11}$$

In Figure 1 we show the magnon spectrum along the direction $q_x = \frac{2\pi}{a}h, q_y = \frac{2\pi}{b}h, q_z = 1.3\frac{2\pi}{c}$ ($(h, h, 1.3)$ direction in r.l.u.) neglecting exchange interactions at all. Inelastic neutron scattering data [4] along the above direction are shown in Figure 1 by open circles. As one can see experimental data *cannot* be recovered. For this reason we have introduced exchange interactions. Figure 2 shows the agreement of our results with the experimental data obtained by the choice $J = 0.030$ meV, $J' = 0.0015$ meV,

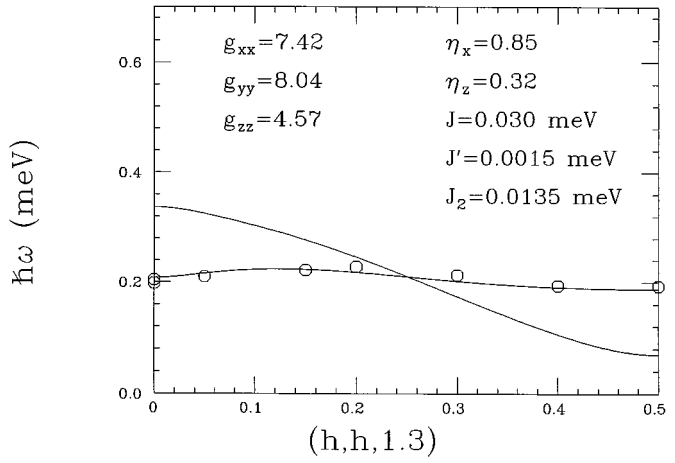

Fig. 2. Dispersion relation along $(h, h, 1.3)$ in r.l.u. taking both dipolar and exchange interactions into account. Open circles are experimental data from reference [4].

$J_2 = 0.0135$ meV. Obviously, this choice satisfies the stability condition $J - 2J_2 < 0.047$ meV given at the end of Section 2. The only effect of a weak J' is to stabilize the antiferromagnetic ordering along the c axis. Even though the best fit is obtained by the above choice, reasonable fitting can be achieved in the range $0.025 < J < 0.035$ meV provided that any increasing of J is joined to a convenient decreasing of J_2. Anyway the introduction of a NNN in-plane antiferromagnetic interaction J_2 which supports columnar ordering, is crucial. As one can see in Figure 2 experimental data fall on a unique curve. In the next Section we will discuss the inelastic neutron scattering cross-section in order to understand why only one branch is observed experimentally. Further experimental data in different directions of the reciprocal lattice as $(h, 0, l)$ or $(0, h, l)$ should be welcome in order to evaluate unambiguously the exchange interactions.

4 Neutron scattering cross-section

Inelastic neutron scattering cross-section is [12]

$$\left(\frac{d^2\sigma}{d\Omega d\omega}\right) \propto |F(\mathbf{q})|^2 \Bigg\{ \left(1 - \frac{q_z^2}{q^2}\right) g_{zz}^2 \sqrt{\frac{A_\mathbf{q} - B_\mathbf{q}}{A_\mathbf{q} + B_\mathbf{q}}} \times \left[(1 + n_\mathbf{q}) \delta(\omega - \omega_\mathbf{q}^+) + n_\mathbf{q} \delta(\omega + \omega_\mathbf{q}^+) \right] + \left(1 - \frac{q_x^2}{q^2}\right) g_{xx}^2 \sqrt{\frac{A_{\mathbf{q}+\mathbf{Q}} + B_{\mathbf{q}+\mathbf{Q}}}{A_{\mathbf{q}+\mathbf{Q}} - B_{\mathbf{q}+\mathbf{Q}}}} \times \left[(1 + n_{\mathbf{q}+\mathbf{Q}}) \delta(\omega - \omega_\mathbf{q}^-) + n_{\mathbf{q}+\mathbf{Q}} \delta(\omega + \omega_\mathbf{q}^-) \right] \Bigg\} \tag{4.1}$$

where $\mathbf{q}$ is the scattering vector. In Table 1 we give the

Table 1. Peak intensity of inelastic neutron scattering and related frequencies (meV) along $(h, h, 1.3)$.

h	$I_\mathbf{q}^+$	$\omega_\mathbf{q}^+$	$I_\mathbf{q}^-$	$\omega_\mathbf{q}^-$
0	0	0.337	48.317	0.208
0.1	2.094	0.303	44.615	0.223
0.2	6.705	0.246	43.583	0.218
0.3	9.597	0.174	41.769	0.202
0.4	8.420	0.105	37.509	0.191
0.5	6.582	0.070	33.968	0.188

peak intensities

$$I_\mathbf{q}^+ = g_{zz}^2 \left(1 - \frac{q_z^2}{q^2}\right) \sqrt{\frac{A_\mathbf{q} - B_\mathbf{q}}{A_\mathbf{q} + B_\mathbf{q}}},$$
$$I_\mathbf{q}^- = g_{xx}^2 \left(1 - \frac{q_x^2}{q^2}\right) \sqrt{\frac{A_{\mathbf{q}+\mathbf{Q}} + B_{\mathbf{q}+\mathbf{Q}}}{A_{\mathbf{q}+\mathbf{Q}} - B_{\mathbf{q}+\mathbf{Q}}}} \tag{4.2}$$

and related frequencies $\omega_\mathbf{q}^+$, $\omega_\mathbf{q}^-$ along the $(h, h, 1.3)$ direction. As one can see the peak intensity $I_\mathbf{q}^-$ is always larger than $I_\mathbf{q}^+$. This could explain the fact that only a branch of the spin wave spectrum is observed experimentally [4]. We recall that the full width at half maximum (FWHM) in experimental data [4] is $\Delta\omega \simeq 0.1$ meV and that a pronounced non magnetic peak is observed around $\omega = 0$. In Figure 3 we simulate the neutron scattering peak profile by the sum of two Gaussians centred at $\omega_\mathbf{q}^+$ and $\omega_\mathbf{q}^-$, according to Table 1, for $\mathbf{q} = (0.1, 0.1, 1.3)$ (3a), $\mathbf{q} = (0.2, 0.2, 1.3)$ (3b), $\mathbf{q} = (0.3, 0.3, 1.3)$ (3c), $\mathbf{q} = (0.4, 0.4, 1.3)$ (3d), respectively. The FWHM of the two Gaussians (open circles) is chosen to be $\Delta\omega = 0.1$ meV according to the energy resolution of the experiment [4]. The areas under the two Gaussians are chosen to be $I_\mathbf{q}^+$ and $I_\mathbf{q}^-$, respectively. Their values are taken from Table 1. Continuous curve is the sum of the two Gaussians. As one can see the unique peak observed in experiment could be explained by the ovrlap of two peaks of different intensities. In this way the experimental data shown in Figure 2 of reference [4] can be recovered. In particular, our Figure 3c compares favorably with experimental peak profile shown in Figure 3a of reference [4]. Note that the peak at $\omega = 0$ observed in experiment is not magnetic in origin so that our calculation has nothing to do with it.

5 Summary and concluding remarks

We have shown that both dipolar and exchange interactions must be taken into account in order to get a reliable description of the magnetic properties of $ErBa_2Cu_3O_7$ [1]. Owing to the in-plane anisotropy of the g-tensor [6], the dipolar interactions are sufficient to explain the ground state spin configuration observed by elastic neutron scattering [1]. However, the exchange interactions, even though very weak, are crucial in order to explain the

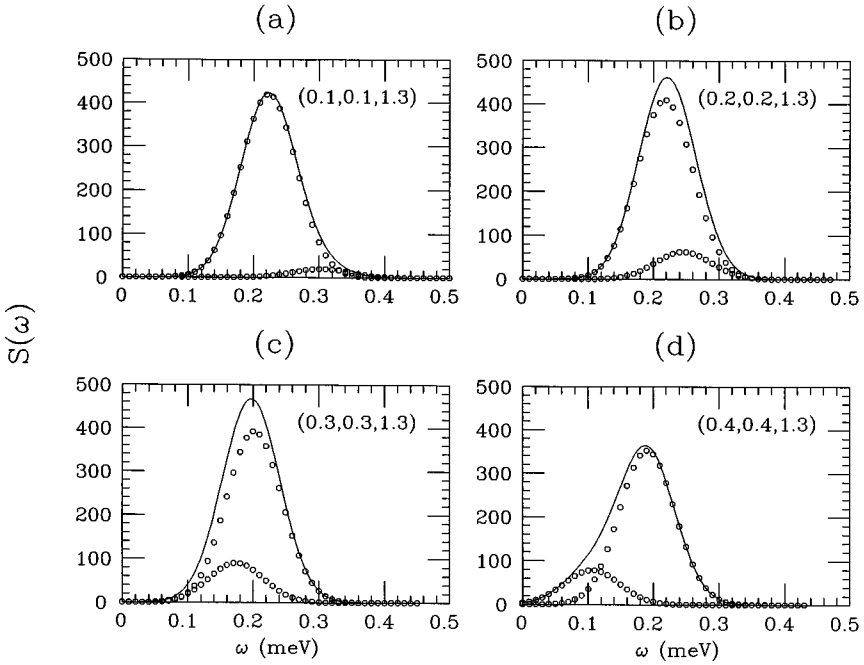

Fig. 3. Peak profile (continuous curve) simulated by the sum two Gaussians (open circles) with FWHM of 0.1 meV centered at ω^+ and ω^- for selected values of **q** along the $(h, h, 1.3)$ direction. (a): $h = 0.1$, (b): $h = 0.2$, (c): $h = 0.3$, (d): $h = 0.4$.

inelastic neutron scattering data [4]. The spin wave spectrum we obtain consists on two branches and the splitting induced by the dipolar interactions is relevant, of the same order of the observed gap [4] along the $(h, h, 1.3)$ direction where the experimental data fall on a unique curve. We have calculated the inelastic neutron cross-section along this direction and we have recovered the experimental data since only one branch is actually observable owing to marked differences between the intensities of the two branches, and the instrumental resolution limitation.

In conclusion we stress that spin waves in $ErBa_2Cu_3O_7$ show features strongly affected by dipolar forces because the exchange is very weak. In this case dipolar forces cannot be simply simulated by a single ion effective anisotropy as it occurs, for instance, in transition metal compounds [5].

This research was supported in part by Consiglio Nazionale delle Ricerche. The authors acknowledge Dr. U. Staub for stimulating correspondence and Prof. G. Amoretti for helpful discussions.

References

1. T.W. Clinton, J.W. Lynn, J.Z. Liu, Y.X. Jia, T.J. Goodwin, R.N. Shelton, B.W. Lee, M. Buchgeister, M.B. Maple, J.L. Peng, Phys. Rev. B **51**, 15429 (1995).
2. S.K. Misra, J. Felsteiner, Phys. Rev. B **46**, 11033 (1992).
3. E. Rastelli, A. Tassi, Physica B **241-243**, 663 (1998).
4. S. Skanthakumar, J.W. Lynn, F. Dogan, J. Appl. Phys. **81**, 4934 (1997).
5. H.W. de Wijn, L.R. Walker, R.E. Walstedt, Phys. Rev. B **8**, 285 (1973).
6. J. Mesot, P. Allenspach, U. Staub, A. Furrer, H. Mutka, R. Osborn, A. Taylor, Phys. Rev. B **47**, 6027 (1993).
7. S. Simizu, G.H. Bellesis, J. Lukin, S.A. Friedberg, H.S. Lessure, S.M. Fine, M. Greenblatt, Phys. Rev. B **39**, 9099 (1989).
8. S.K. Misra, Y. Chang, J. Felsteiner, J. Phys. Chem. Solids, **58**, 1 (1997).
9. F. Keffer, *Handbuck der Physik* (Springer, New York, 1966) Vol. XVIII/2, p. 1.
10. C. Pich, F. Schwabl, Phys. Rev. B **47**, 7957 (1993).
11. M. Baehr, M. Winkelmann, P. Vorderwisch, M. Steiner, C. Pich, F. Schwabl, Phys. Rev. B **54**, 12932 (1996).
12. S.W. Lovesey, *Theory of neutron scattering from condensed matter* (Clarendon Press, Oxford, 1984) Vol. 2, p. 256.